

# Productivity of North American grasslands is increased under future climate scenarios despite rising aridity

Koen Hufkens<sup>1\*</sup>, Trevor F. Keenan<sup>2</sup>, Lawrence B. Flanagan<sup>3</sup>, Russell L. Scott<sup>4</sup>, Carl J. Bernacchi<sup>5,6</sup>, Eva Joo<sup>5</sup>, Nathaniel A. Brunsell<sup>7</sup>, Joseph Verfaillie<sup>8</sup> and Andrew D. Richardson<sup>1\*</sup>

**Grassland productivity is regulated by both temperature and the amount and timing of precipitation<sup>1,2</sup>. Future climate change is therefore expected to influence grassland phenology and growth, with consequences for ecosystems and economies. However, the interacting effects of major shifts in temperature and precipitation on grasslands remain poorly understood and existing modelling approaches, although typically complex, do not extrapolate or generalize well and tend to disagree under future scenarios<sup>3,4</sup>. Here we explore the potential responses of North American grasslands to climate change using a new, data-informed vegetation-hydrological model, a network of high-frequency ground observations across a wide range of grassland ecosystems and CMIP5 climate projections. Our results suggest widespread and consistent increases in vegetation fractional cover for the current range of grassland ecosystems throughout most of North America, despite the increase in aridity projected across most of our study area. Our analysis indicates a likely future shift of vegetation growth towards both earlier spring emergence and delayed autumn senescence, which would compensate for drought-induced reductions in summer fractional cover and productivity. However, because our model does not include the effects of rising atmospheric CO<sub>2</sub> on photosynthesis and water use efficiency<sup>5,6</sup>, climate change impacts on grassland productivity may be even larger than our results suggest. Increases in the productivity of North American grasslands over this coming century have implications for agriculture, carbon cycling and vegetation feedbacks to the atmosphere.**

The grassland biome is the largest in the world, covering up to 59 million km<sup>2</sup> (over 30% of the global land surface)<sup>1</sup>. Grasslands constitute a key component of the terrestrial biosphere and are fundamental to the meat and dairy industries<sup>1</sup>, but projections of grassland growth and productivity from model intercomparison studies diverge greatly under climate change<sup>3,4</sup>.

Grassland growth and productivity are highly dynamic on fast (days-to-weeks) timescales, leading to substantial variability between years<sup>7–9</sup>. Grassland growth is largely controlled by soil water content and the magnitude, frequency and timing of precipitation events<sup>10–12</sup>. The response of grasslands to changes in precipitation

varies between ecosystems<sup>13,14</sup>, as available soil water is also driven by interactions between soil water potential, atmospheric demand and the physiology of individual plant species. This argues for the use of mechanistic grassland ecosystem models<sup>14,15</sup>, which should be developed and tested using high-frequency observations, rather than more aggregated measures (for example, annual productivity), so that fast growth dynamics can be adequately characterized. High-frequency eddy-covariance measurements of ecosystem–atmosphere CO<sub>2</sub> exchange have been previously used to test grassland models<sup>14–16</sup>. Although such measurements contain information on photosynthesis and respiration<sup>17</sup>, they cannot be used directly to constrain important ecosystem state variables such as biomass or fractional cover (fCover, the proportion of ground area covered by green foliage).

Here we develop a coupled vegetation-hydrological model<sup>18</sup> to predict daily changes in grassland fCover, based on growth and senescence relationships that depend on both the prevailing meteorology and modelled soil hydrology. We constrain the model parameterization with daily measures of vegetation greenness (in terms of  $G_{cc}$ , the green chromatic coordinate), derived from 34 site-years of PhenoCam network imagery<sup>19</sup> (Fig. 1). We independently validate model predictions using 28 years of aboveground net primary productivity (ANPP) data from the Konza Prairie Biological Station and satellite-derived fCover.

We use the model to predict the response of grassland productivity to changes in temperature and precipitation as projected by 10 downscaled Coupled Model Intercomparison Project Phase 5 (CMIP5) climate projections for a business-as-usual scenario (Representative Concentration Pathway (RCP) 8.5). The results indicate widespread increases in grassland fCover over the coming century across the majority of North American grasslands despite increased aridity (Fig. 2b)<sup>20</sup>, with shifts in the growth of grasslands in spring and autumn broadly compensating for drought-induced declines in summer.

Simultaneous optimization of the model to PhenoCam data from 14 North American grassland sites (Supplementary Fig. 1) showed that a single set of parameters adequately captured the timing, magnitude and rate of grassland growth and senescence (that is, changes in fCover) across a wide range of climate zones

<sup>1</sup>Department of Organismic and Evolutionary Biology, Harvard University, Cambridge, Massachusetts 02138, USA. <sup>2</sup>Department of Biological Sciences, Macquarie University, Sydney, New South Wales 02109, Australia. <sup>3</sup>Department of Biological Sciences, University of Lethbridge, Lethbridge, Alberta T1K3M4, Canada. <sup>4</sup>Southwest Watershed Research Center, USDA-ARS, Tucson, Arizona 85719, USA. <sup>5</sup>Department of Plant Biology, University of Illinois, Urbana, Illinois 61801, USA. <sup>6</sup>USDA-ARS, Global Change and Photosynthesis Research Unit, Urbana, Illinois 61801, USA. <sup>7</sup>Department of Geography and Atmospheric Sciences, University of Kansas, Lawrence, Kansas 66045, USA. <sup>8</sup>Department of Environmental Science, Policy and Management, University of California-Berkeley, Berkeley, California 94720, USA. \*e-mail: koen.hufkens@gmail.com; arichardson@oeb.harvard.edu

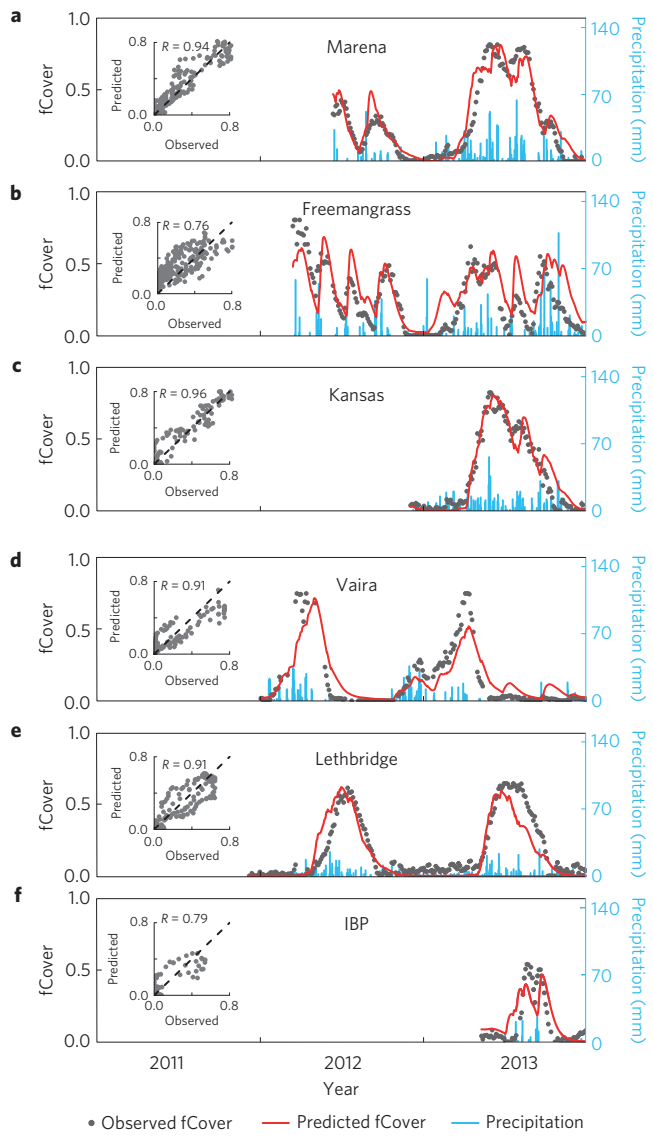


**Figure 1 | Observed and predicted fCover time series for six sites in various climate regimes and with different growth dynamics.** Six time series of PhenoCam observed and model predicted grassland fCover using the global optimal parameter set as black dots and a full red line respectively. Precipitation is shown as blue vertical bars. Inset graphs show scatterplots and the Pearson correlation coefficient of observed and predicted fCover. Site names as mentioned on top of each panel correspond to those in Supplementary Table 1. See Supplementary Fig. 3 for all sites. Time series are ordered from humid to arid climate conditions. **a,b**, Two examples of a humid subtropical climate (Koppen-Geigen classification Cfa) from Marena (**a**) and Freemangrass (**b**). **c**, A humid warm summer continental climate (Dfa). **d**, A Mediterranean climate (Csb). **e**, A humid mild summer continental climate (Dfb). **f**, A semi-arid or steppe climate (Bsk). IBP, a site of the US GrasslandBiome project of the International Biological Program.

(Fig. 1 and Supplementary Table 1). For example, the model captured the rapid response of grasslands dominated by  $C_4$  species to precipitation pulses in both humid subtropical (Fig. 1a,b), humid warm continental (Fig. 1c) and Mediterranean (Fig. 1d) climates, and also reproduced the multiple growth cycles occurring within a single year at those sites. Similarly, the model effectively captured both the timing and magnitude of fCover dynamics at grasslands with humid mild summer continental climates (Fig. 1e), where  $C_3$  species predominate and there is typically just a single annual growth cycle. Across all sites the model explained 75%

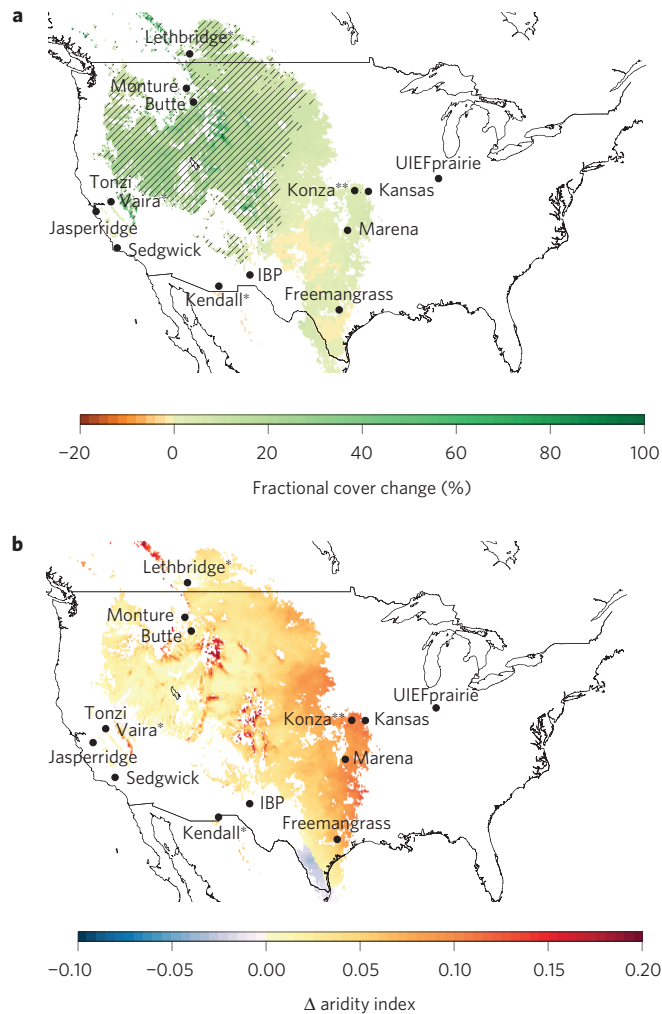


**Figure 2 | Predicted changes in grassland fCover and aridity at the end of the century.** **a,b**, Contrasting the change in percentage mean total annual grassland fCover between the end (2090–2100) and the start (2010–2020) of the twenty-first century (**a**), with changes in the median difference ( $\Delta$ ) in annual aridity between the start (2010–2020) and the end (2090–2100) of the twenty-first century (**b**) for the ensemble mean across the ten climate scenarios used in this study. Areas with a significant trend ( $p < 0.05$ ) in grassland fCover over the next century for at least half of the model scenarios are indicated by diagonal hatching. Aridity is expressed as the ratio of mean annual precipitation and mean annual potential evapotranspiration. Increases in the aridity index signify increased aridity. PhenoCam locations (black filled circle) where ecosystem flux data were available are marked with single black asterisks (\*). Locations where further structural parameters (biomass) were available are marked by two black asterisks (\*\*).

of the observed temporal variability in daily fCover ( $p < 0.001$ , RMSE = 0.17), and we obtained essentially comparable results ( $71 \pm 19\%$ , mean  $\pm 1$  s.d., across sites) in a leave-one-out cross-validation exercise. When independently validated with satellite-based estimates, the model explained, on average, 61% of the temporal variability in fCover ( $p < 0.001$ , RMSE = 0.16).

We projected future trends in fCover to the year 2100, using an ensemble of climate scenarios. Despite uncertainties in the precipitation projections of different climate models, the ensemble trend in fCover was positive over most of the study area, with the majority of climate model projections in agreement in terms of both the sign and magnitude of the response. Our results indicate significant increases (one-sample  $t$ -test,  $H_0: \mu = 0, p < 0.001$ ) in

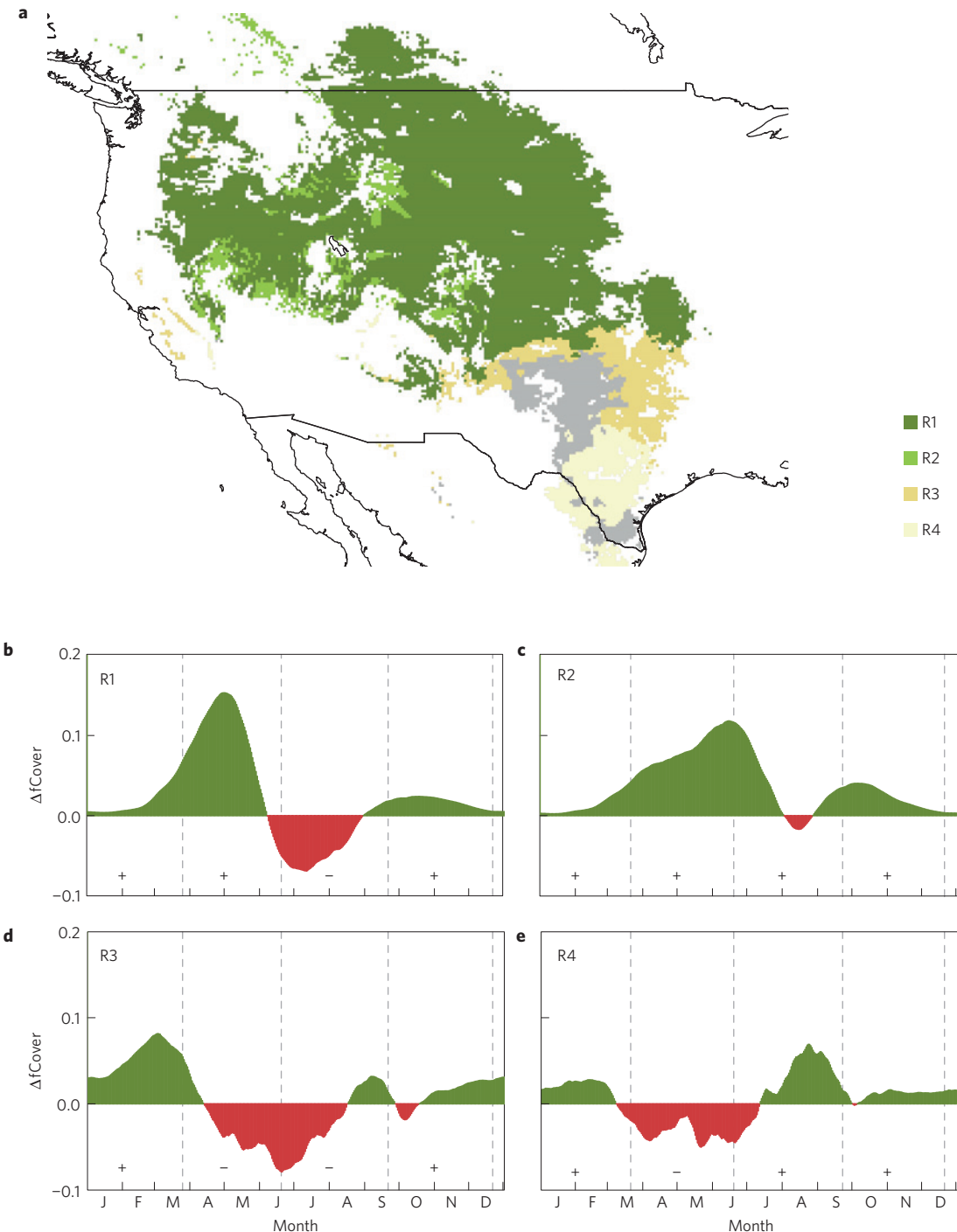


**Figure 3 | Spatial and temporal patterns for four scenarios of changes of grassland fCover by the end of the twenty-first century.** Spatial and temporal profiles in changes in grassland fCover between the end (2090–2100) and the start (2010–2020) of the century for the ensemble mean of the ten CMIP5 climate projections as used in this study. **a**, The regional groupings of the spatial distribution of pixels described by four possible regional grouping scenarios (R1–R4), accounting for 90% of the study area. Areas that do not match any of the four prescribed regional groupings are marked with grey. **b–e**, Mean daily changes in grassland fCover across the four regional groupings (R1–R4) between the end and start of the century for all pixels across a regional grouping. Meteorological seasons are marked with vertical dashed grey lines. Plus and minus signs indicate the direction of the integrated change in fCover across the season as used in the regional grouping.

the integrated annual grassland fCover of  $18 \pm 14/9\%$  across the grassland ecosystems in North America (we report the ensemble mean  $\pm 1$  s.d./1 s.d., where the first is the standard deviation of the spatial mean across the 10 climate scenarios, and the second is the standard deviation of the ensemble mean of the climate scenarios across all modelled grid cells).

The overall trend in fCover varied among regions (Fig. 2a and Supplementary Fig. 12). Regional patterns were typically, but not always, driven by trends in precipitation (Supplementary Fig. 9). However, the combined effect of temperature-driven evaporation and changes in precipitation frequency (Supplementary Table 3) and intensity (Supplementary Figs 9–11) is an increase

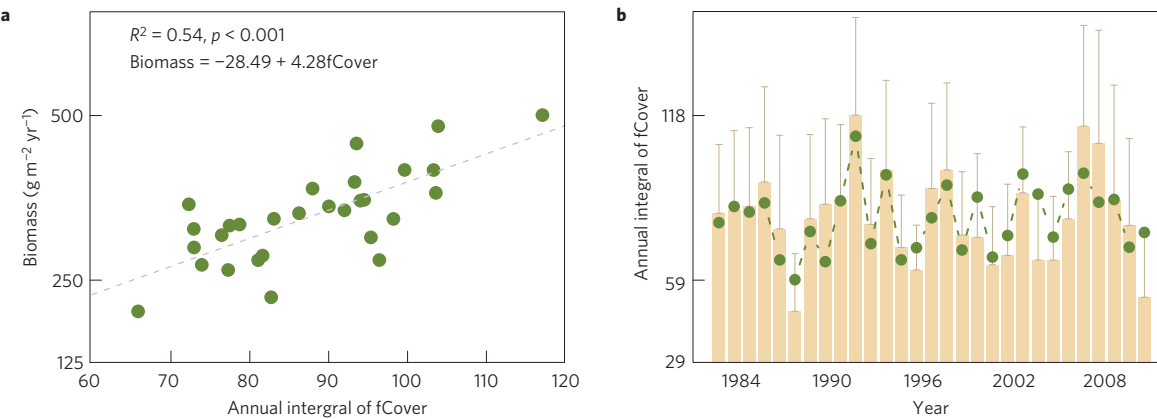


**Figure 4 | Modelled annual fCover and ANPP of tallgrass prairie.** ANPP values are based on accumulated herbaceous plant biomass on Florence soils at the Konza Prairie Biological Station. **a**, The relation between modelled annual fCover and mean measured ANPP. We report a fitted ordinary least squares regression shown as a grey dashed line ( $R^2 = 0.54$ ,  $p < 0.001$ ). **b**, The barplot shows the mean measured ANPP (error bars depict  $\pm 1$  s.d., between plots) in relation to the modelled (green dots) annual fCover values at the Konza Prairie Biological Station.

in aridity<sup>20</sup> (Fig. 2b). Yet, significant increases in total annual fCover were most evident in semi-arid northern grasslands, which accounted for 55% ( $\sim 1.4$  million km $^2$ ) of the study area. In these regions, the climate model ensemble projected increases of  $4.8 \pm 0.9/0.3$  °C in mean annual temperature, and  $44 \pm 78/34$  mm in mean annual precipitation.

Importantly, changes in annual fCover were also accompanied by distinct changes in grassland seasonality. We identified four discrete regional groupings (Fig. 3): R1 includes only areas that exhibit summer reductions in fCover; R2 includes areas with consistent increases in growth throughout the whole growing season; and R3 and R4 include regions with reduced spring and summer growth, but increased winter and fall growth.

Seasonal changes were most evident across regions R1 and R2, which showed shifts in both the timing and magnitude of grassland growth during the shoulder seasons (Fig. 3). For example, for R1 grasslands in the northern part of the study area, a warmer and wetter winter and spring led to earlier peak productivity (Supplementary Table 2). For higher-altitude northern grasslands (R2) the increase in modelled fCover during early summer more than compensated for a negligible mid-summer decline in fCover. On average, the start of grassland growth in spring moved forward by  $21 \pm 7/4$  days and  $25 \pm 8/3$  days for R1 and R2 respectively, where the end of the growing season was postponed  $8 \pm 13/5$  and  $13 \pm 18/5$  days. Thus for R1 and R2, our model indicates an increase in growing season length of up to  $\sim 5$  weeks by 2100.

In contrast, for grasslands in the southern part of the study area (R3 and R4), our model indicates decreases in fCover throughout spring and summer, with only slight increases in late summer, autumn and winter (Fig. 3, R3–R4). This decrease in fCover is associated with projected decreases of up to  $25 \pm 38/9$  mm in spring precipitation (Supplementary Table 3). Summer precipitation increases are counteracted by the concomitant increase in temperature and evaporation, resulting in further decreases in fCover. As such, increases in fCover in southern regions in winter and autumn were offset by decreases in fCover during spring and summer. Overall, there is no statistically significant change in total annual fCover projected for regions R3 and R4.

Grassland phenology, seasonal variation in fCover and annual productivity are all strongly interconnected<sup>7,21</sup>. For example, 28 years of biomass clippings at the Konza Prairie Biological Station show a significant linear relationship with modelled fCover ( $R=0.74$ ,  $p < 0.001$ , Fig. 4). Our model captures the impacts of both short-term droughts and long-term decadal trends, incrementally better than previous studies<sup>22,23</sup>. Moreover,

in subalpine shortgrass ecosystems as well as tallgrass prairie, PhenoCam-derived metrics of vegetation greenness were highly correlated with gross primary productivity (GPP) as estimated from eddy-covariance measurements<sup>24,25</sup>. Yet distinct relations were found between shortgrass and tallgrass sites, showing higher yields for the latter ( $R^2 = 0.86$ ,  $p < 0.001$ ,  $R^2 = 0.83$  and  $p < 0.001$  respectively, Supplementary Fig. 4). At the Lethbridge site, using a conservative shortgrass regression-based estimate, we calculated a mean increase in annual GPP of  $76 \pm 77$  g C m $^{-2}$  (mean  $\pm 1$  s.d., across all climate models) by 2100. This represented a 15% increase in annual GPP over current estimates ( $502 \pm 240$  g C m $^{-2}$ ; 12 year mean  $\pm 1$  s.d., 1999 to 2013; ref. 26). The projected average growing season increase of  $4 \pm 2$  weeks (mean  $\pm 1$  s.d., across all climate models) at the Lethbridge site suggests an increase in annual GPP of between  $56 \pm 29$  g C m $^{-2}$  and  $140 \pm 72$  g C m $^{-2}$ . Our regression-based estimate falls at the lower end of this range, because it accounts for the influence of changes in both growing season length as well as summer droughts on GPP.

Applying the conservative shortgrass regression-based estimate across the current range of grassland ecosystems in North America, the ensemble trend in GPP was positive over 89% of the study area (Supplementary Figs 1 and 7). And, both the sign and magnitude of the GPP response to future climate change was consistent across most climate models. Thus, our model results indicate increases in the total annual grassland GPP (annual productivity estimated as fCover scaled to GPP) of  $52 \pm 55/38$  g C m $^{-2}$  or  $0.11 \pm 0.08$  Pg (76  $\pm 57/28$  g C m $^{-2}$  or  $0.08 \pm 0.06$  Pg C, for the areas with a significant change).

Experimental evidence suggests that future elevated CO<sub>2</sub>, which is not included in our model, should also increase grassland productivity (in the absence of nutrient limitations<sup>27</sup>) and growing season length through species complementarity<sup>5</sup> and increased water use efficiency<sup>6</sup>, limiting water losses through transpiration and thereby increasing available soil water. In an earlier manipulative experiment conducted in a temperate grassland, growing season extension was most pronounced when warming was combined with elevated CO<sub>2</sub>, because water conservation allowed plants to remain active longer<sup>6</sup>. However, the effect of CO<sub>2</sub> is likely to depend on ecosystem composition<sup>28</sup> and temporal changes in the principal drivers<sup>12,29</sup> (Supplementary Table 3). A mechanistic and generalized understanding of these complex effects of CO<sub>2</sub> on grassland fCover is still lacking. Our model projections do not account for the effects of CO<sub>2</sub> on productivity through increases in photosynthesis and water use efficiency<sup>6</sup>. Our results therefore probably represent an

underestimate of the potential growth response of grasslands to future climate change<sup>28</sup>.

Our modelling analysis suggests widespread changes in both the timing and magnitude of North American grassland growth and productivity in response to future climate change (Supplementary Figs 8–11). Overall, our projections indicate significant gains ( $18 \pm 14\%$ ) in grassland fCover by 2100 across more than half of the region that is dominated by grasslands at present. Furthermore, we find substantial increases in growing season length (by ~5 weeks) across much of this biome. Together, these results have large implications for agricultural productivity, biophysical feedbacks to the climate system and terrestrial carbon cycling<sup>26,30</sup>.

## Methods

Methods and any associated references are available in the online version of the paper.

Received 13 April 2015; accepted 20 January 2016;  
published online 29 February 2016

## References

- Parton, W. *et al.* Impact of precipitation dynamics on net ecosystem productivity. *Glob. Change Biol.* **18**, 915–927 (2012).
- Peng, S., Piao, S., Shen, Z., Ciais, P. & Sun, Z. Precipitation amount, seasonality and frequency regulate carbon cycling of a semi-arid grassland ecosystem in Inner Mongolia, China: A modeling analysis. *Agric. For. Meteorol.* **178–179**, 46–55 (2013).
- Hillel, D. & Rosenzweig, C. *Handbook of Climate Change and Agroecosystems: The Agricultural Model Intercomparison and Improvement Project (AgMIP) Integrated Crop and Economic Assessments* (Imperial College Press, 2015).
- Dong, J. *et al.* Comparison of four EVI-based models for estimating gross primary production of maize and soybean croplands and tallgrass prairie under severe drought. *Remote Sens. Environ.* **162**, 154–168 (2015).
- Reyes-Fox, M. *et al.* Elevated CO<sub>2</sub> further lengthens growing season under warming conditions. *Nature* **510**, 259–262 (2014).
- Morgan, J. A. *et al.* C<sub>4</sub> grasses prosper as carbon dioxide eliminates desiccation in warmed semi-arid grassland. *Nature* **476**, 202–205 (2011).
- Flanagan, L. B. & Adkinson, A. C. Interacting controls on productivity in a northern Great Plains grassland and implications for response to ENSO events. *Glob. Change Biol.* **17**, 3293–3311 (2011).
- Gilmanov, T. G. *et al.* Partitioning European grassland net ecosystem CO<sub>2</sub> exchange into gross primary productivity and ecosystem respiration using light response function analysis. *Agric. Ecosyst. Environ.* **121**, 93–120 (2007).
- Ma, S., Baldocchi, D. D., Xu, L. & Hehn, T. Inter-annual variability in carbon dioxide exchange of an oak/grass savanna and open grassland in California. *Agric. For. Meteorol.* **147**, 157–171 (2007).
- Huxman, T. E. *et al.* Precipitation pulses and carbon fluxes in semiarid and arid ecosystems. *Oecologia* **141**, 254–268 (2004).
- Knapp, A. K. & Smith, M. D. Variation among biomes in temporal dynamics of aboveground primary production. *Science* **291**, 481–485 (2001).
- Knapp, A. K. *et al.* Rainfall variability, carbon cycling, and plant species diversity in a mesic grassland. *Science* **298**, 2202–2205 (2002).
- Knapp, A. K. *et al.* Consequences of more extreme precipitation regimes for terrestrial ecosystems. *Bioscience* **58**, 811–821 (2008).
- Chang, J. *et al.* Incorporating grassland management in a global vegetation model: model description and evaluation at 11 eddy-covariance sites in Europe. *Geosci. Model Dev. Discuss.* **6**, 2769–2812 (2013).
- Ciais, P., Soussana, J. F., Vuichard, N., Luysaert, S. & Don, A. The greenhouse gas balance of European grasslands. *Biogeosciences* **7**, 5997–6050 (2010).
- Zhang, L. *et al.* Upscaling carbon fluxes over the Great Plains grasslands: sinks and sources. *J. Geophys. Res. Biogeosci.* **116**, 1–13 (2011).
- Schwalm, C. R. *et al.* Reduction in carbon uptake during turn of the century drought in western North America. *Nature Geosci.* **5**, 551–556 (2012).
- Choler, P., Sea, W., Briggs, P., Raupach, M. & Leuning, R. A simple ecohydrological model captures essentials of seasonal leaf dynamics in semi-arid tropical grasslands. *Biogeosciences* **7**, 907–920 (2010).
- Richardson, A. D., Braswell, B. H., Hollinger, D. Y., Jenkins, J. P. & Ollinger, S. V. Near-surface remote sensing of spatial and temporal variation in canopy phenology. *Ecol. Appl.* **19**, 1417–1428 (2009).
- Seager, R. *et al.* Projections of declining surface-water availability for the southwestern United States. *Nature Clim. Change* **3**, 482–486 (2012).
- Running, S. W. *et al.* A continuous satellite-derived measure of global terrestrial primary production. *Bioscience* **54**, 547–560 (2004).
- Del Grosso, S. Global potential net primary production predicted from vegetation class, precipitation, and temperature. *Ecology* **89**, 2117–2126 (2008).
- Sala, O. E., Parton, W. J., Joyce, L. A. & Lauenroth, W. K. Primary production of the central grassland region of the United States. *Ecology* **69**, 40–45 (1988).
- Toomey, M. *et al.* Greenness indices from digital cameras predict the timing and seasonal dynamics of canopy-scale photosynthesis. *Ecol. Appl.* **25**, 99–115 (2015).
- Migliavacca, M. *et al.* Using digital repeat photography and eddy covariance data to model grassland phenology and photosynthetic CO<sub>2</sub> uptake. *Agric. For. Meteorol.* **151**, 1325–1337 (2011).
- Flanagan, L. B., Sharp, E. J. & Gamon, J. A. Application of the photosynthetic light-use efficiency model in a northern Great Plains grassland. *Remote Sens. Environ.* **168**, 239–251 (2015).
- Reich, P. B. *et al.* Nitrogen limitation constrains sustainability of ecosystem response to CO<sub>2</sub>. *Nature* **440**, 922–925 (2006).
- Reeves, M. C., Moreno, A. L., Bagné, K. E. & Running, S. W. Estimating climate change effects on net primary production of rangelands in the United States. *Climatic Change* **126**, 429–442 (2014).
- Fay, P. A. *et al.* Relative effects of precipitation variability and warming on tallgrass prairie ecosystem function. *Biogeosciences* **8**, 3053–3068 (2011).
- Richardson, A. D. *et al.* Climate change, phenology, and phenological control of vegetation feedbacks to the climate system. *Agric. For. Meteorol.* **169**, 156–173 (2013).

## Acknowledgements

The Richardson Lab acknowledges support from the NSF Macrosystems Biology programme (award EF-1065029). T.F.K. acknowledges support from a Macquarie University research fellowship. The Lethbridge ecosystem flux measurements were supported by Discovery grants from the Natural Sciences and Engineering Research Council of Canada to L.B.F. (RGPIN-2014-05882). We thank the World Climate Research Program's Working Group on Coupled Modelling, which is responsible for CMIP, and we thank the climate modelling groups (listed in Supplementary Table 6) for producing and making available their model output. For CMIP the US Department of Energy's Program for Climate Model Diagnosis and Inter-comparison provides coordinating support and led development of software infrastructure in partnership with the Global Organization for Earth System Science Portals. Furthermore, we acknowledge the Downscaled CMIP3 and CMIP5 Climate and Hydrology Projections archive hosted at [http://gdo-dcp.ucllnl.org/downscaled\\_cmip\\_projections](http://gdo-dcp.ucllnl.org/downscaled_cmip_projections) for making their data available. We thank X. Xiao for providing data from the Marena, Oklahoma, site acquired through research grants from the USDA NIFA (Project No. 2012-02355) and National Science Foundation (IAA-1301789). Research at the Continental Divide PhenoCam Site in Butte, Montana is supported by the National Science Foundation-EPSCoR (grant NSF-0701906), OpenDap and Montana Tech of the University of Montana. The Jasper Ridge Biological Preserve is supported by Stanford University and the Carnegie Institution Department of Global Ecology. Research at the Kendall site, Walnut Gulch Experimental Watershed, is funded by the USDA-ARS and the US Department of Energy. Data for PAB01 (Aboveground net primary productivity of tallgrass prairie based on accumulated plant biomass on core LTER watersheds) and climate data (AWE01, APT01) was supported by the NSF Long Term Ecological Research Program (LTER) at the Konza Prairie Biological Station. N.A.B. acknowledges support from the LTER programme at the Konza Prairie Biological Station (DEB-0823341), where the US-Kon Ameriflux site is sponsored by the US Department of Energy under a sub contract from DE-AC02-05CH11231. We thank T. Milliman for maintenance of the PhenoCam data archive, and our PhenoCam collaborators for their efforts in support of this project.

## Author contributions

K.H. and A.D.R. designed the study and methodology, with input from T.F.K. A.D.R. contributed PhenoCam imagery. K.H. processed the imagery and performed model simulations. L.B.F., R.L.S., C.J.B., E.J., N.A.B. and J.V. contributed ecosystem flux data. All authors contributed to data analysis and interpretation. K.H. drafted the manuscript with input from T.F.K. and A.D.R. All authors commented on and approved the final manuscript.

## Additional information

Supplementary information is available in the online version of the paper. Reprints and permissions information is available online at [www.nature.com/reprints](http://www.nature.com/reprints). Correspondence and requests for materials should be addressed to K.H. or A.D.R.

## Competing financial interests

The authors declare no competing financial interests.

## Methods

**PhenoCam data.** The PhenoCam network uses digital camera imagery to monitor ecosystem dynamics at a fine spatial and temporal resolution. These near-surface remote sensing images are processed using a simple image analysis techniques to extract quantitative colour information of vegetation greenness ( $G_{cc}$ ; ref. 31) for an appropriate region of interest (ROI), providing daily information on the amount of foliage present and its colour<sup>32</sup>. We selected 14 PhenoCam grassland sites (Fig. 1, Supplementary Fig. 2 and Supplementary Table 1), with 34 site-years of data, spread across North America. PhenoCam imagery for all sites was processed into normalized (0–1)  $G_{cc}$  time series. These  $G_{cc}$  time series, capturing the relative amplitude in vegetation growth, were scaled to an fCover range. We use an asymptotic transfer function, based on the nonlinear relationship between fCover and MAP (ref. 33), to calculate a scaling factor ( $S_c$ ) using:

$$S_c = \text{MAP}/(\text{MAP} + h) \quad (1)$$

where MAP is mean annual precipitation, and  $h$  is the steepness of the asymptotic curve estimated during optimization taking into account all available site-years.

**Model description.** The ‘PhenoGrass’ model is a coupled soil moisture and vegetation model. The model captures plant–soil moisture dynamics using nonlinear relationships between available soil water and vegetation. The model is based on a previously published formulation<sup>18</sup> but uses a daily time step and a temperature response function (equation (10)) to account for rapid changes in (temperature-dependent) growth conditions, expanding the model outside its original extent.

In the PhenoGrass model we estimate both soil water content ( $W_t$ , equation (2)) and grassland fCover ( $V_t$ , equation (3)) at a daily time step ( $t$ ). Nonlinear changes in grassland fCover are controlled by a vegetation growth parameter ( $b_1$ ), a temperature response factor ( $g$ ), a light response function depending on top-of-atmosphere (TOA) radiation ( $S_t$ , equation (8)) and lagged plant available water ( $D_{t-1}$ ). Similarly, a nonlinear response describes losses in fCover that are mediated by a senescence factor ( $b_2$ ) when plant available water or available light is decreasing (equation (7),  $d=1$ ). The status of  $W_t$  depends on inputs from precipitation ( $P_t$ ) and losses through evaporation ( $E_t$ ), transpiration and runoff.

We model evaporation losses as the bare soil fraction, dependent on the relative soil water content ( $D_t/(W_{cap} - W_p)$ )<sup>2</sup> or the squared ratio of the current plant available water ( $D_t$ ), the difference between the current soil water status and ( $W_t$ ) and the wilting point, and maximum ( $W_{cap} - W_p$ ) soil water content, with  $W_{cap}$  and  $W_p$  the field capacity and wilting point, respectively. Plant transpiration is a water- and temperature-limited process, dependent on  $D_t$ , the soil water extraction rate ( $b_3$ ) and a temperature response<sup>34</sup> ( $g$ , equation (10)) limiting transpiration in unfavourable conditions. All precipitation accumulation exceeding field capacity runs off (equation (5)). Values for the soil field capacity and wilting point were extracted from the global homogenized soil profile data set<sup>35</sup>. Evapotranspiration ( $E_t$ ) is calculated according to the Hargreaves equation<sup>36</sup>.

Where the PhenoGrass model can be summarized as:

$$W_{t+1} = W_t + P_t - (1 - V_t)(D_t / (W_{cap} - W_p))^2 E_t - g b_3 D_t \quad (2)$$

$$V_{t+1} = V_t + g S_t b_1 D_{t-1} (1 - V_t / V_{max}) - d b_2 (1 - V_t) * V_t \quad (3)$$

With

$$D_t = \max(0, W_t - W_p) \quad (4)$$

$$W_t = \max(0, \min(W_{cap}, W_t)) \quad (5)$$

$$V_t = \max(0, \min(V_{max}, V_t)) \quad (6)$$

$$\begin{cases} D_{t-1} > D_{t-1-1}; & d = 0 \\ D_{t-1} \leq D_{t-1-1}; & d = 1 \end{cases} \quad (7)$$

$$S_t = (\text{TOA}_r - \text{Phmin}) / (\text{Phmax} - \text{Phmin}) \quad (8)$$

$$\begin{cases} S_{t-1} > S_t; & d = 1 \\ S_{t-1} \leq S_t; & d = 0 \end{cases} \quad (9)$$

The temperature response function accounts for rapid changes in (temperature-dependent) growth conditions and is defined as:

$$g = \left( \frac{T_{max} - T_m}{T_{max} - T_{opt}} \right) \left( \frac{T_m}{T_{opt}} \right)^{\left( \frac{T_{opt}}{T_{max} - T_{opt}} \right)} \quad (10)$$

with  $T_{max}$  set at 45 °C,  $T_m$  is the running mean air temperature for the previous 15 days and  $T_{opt}$  is the optimal temperature, obtained in the process of optimizing  $g$  as

part of the global model parameter set. TOA radiation (TOA<sub>r</sub>) is calculated according to ref. 37 and scaled between 0–1 using parameters Phmin and Phmax (equation (8)), where 0 inhibits growth and 1 allows for full growth. Declining radiation trends enforce senescence even under favourable soil water conditions (equation (9)).

**Model optimization.** Time series of vegetation greenness were assimilated to constrain model parameterization. All model parameters and the vegetation greenness scaling parameter ( $h$ ) were estimated during optimization. We optimized global model parameters (that is, for all sites simultaneously with Daymet<sup>38</sup> climate drivers) using a Markov Chain Monte Carlo approach<sup>39</sup>, repeating the optimization process with random initial input values and minimizing a cost function ( $F$ ) defined as the mean coefficient of variation of the mean absolute error<sup>16</sup> using all  $G_{cc}$  time series (equation (11)). Preceding years were used as a spin-up period to equilibrate the soil water pool. A leave-one-out cross-validation was executed, keeping parameter ‘ $h$ ’ constant. We report cross-validated parameter estimates and their uncertainties as well as the mean and standard deviation of the  $R^2$  and RMSE across all sites (Supplementary Table 5).

$$F = \frac{1}{N} \sum_{j=1}^N \text{CVMAE}_j \quad (11)$$

with

$$\text{CVMAE}_j = \left( \sum_{i=1}^n |\text{fCover}_{i,\text{obs}} - \text{fCover}_{i,\text{pred}}| \right) / \overline{\text{fCover}}_{\text{obs}}$$

With  $N$  and  $n$  the number of sites and time series values respectively. Where  $\text{fCover}_{i,\text{pred}}$  and  $\text{fCover}_{i,\text{obs}}$  are the predicted and observed fCover values for site  $j$  and sample  $i$ ; and  $\overline{\text{fCover}}_{\text{obs}}$  is the mean observed fCover value for site  $j$ .

Validation was provided by comparing model results, using local climate drivers (AWE01, APT01), with 30 years of end-of-season non-woody biomass measurements (g C m<sup>-2</sup>, PAB01, Fl-soil) at the Konza Prairie Biological Station (<http://www.konza.ksu.edu>). In addition, model results, using Daymet<sup>38</sup> climate drivers, were compared with MODIS (MODerate resolution Imaging Spectrometer) normalized difference vegetation index (NDVI)-based fCover values<sup>40</sup>. We extracted NDVI fCover time series at 100 random homogeneous grassland locations (Supplementary Fig. 1; MOD09A1, tile h10v04, retaining pixels with ideal product quality—QA bit 00) informed by MODIS Land Cover (MCD12Q1) data and validated by visual inspection using Google Earth.

**Ecosystem fluxes.** Eddy-covariance measurements of net ecosystem CO<sub>2</sub> exchange (NEE) were made at 3 shortgrass and 2 tallgrass sites (Lethbridge, Vaira<sup>41</sup>, Kendall, Konza and UIEPrairie; Supplementary Table 1 and Supplementary Fig. 1). With the exception of the UIEPrairie site, which is harvested and has aboveground litter removed, all sites are native or restored, lightly grazed and unmanaged grasslands. Measured NEE values were partitioned into total ecosystem respiration (TER) and GPP using standard protocol for gap filling and partitioning eddy-covariance CO<sub>2</sub> fluxes. At the Lethbridge site the standard Fluxnet-Canada protocols<sup>42</sup> were used, whereas all other sites used the standardized methodology as described in ref.<sup>43</sup>. The GPP values were calculated as the sum of NEP (= –NEE) and TER (that is, GPP = NEP + TER). Meteorological instruments used to monitor environmental conditions have been described previously<sup>41,44–47</sup>.

We use a linear model to describe the relationship between PhenoCam-derived grassland fCover and ecosystem flux measurements of GPP at the shortgrass sites Lethbridge, Kendall and Vaira. Regression parameters were used to estimate the difference in total annual GPP between the start and the end of our CMIP5 projections. Furthermore, previous studies have shown that an increase in growing season length can account for much of the observed annual variation in grassland productivity, with an extended growing season increasing GPP at rates of 2–5 g C m<sup>-2</sup> d<sup>-1</sup> (refs 5,47). We extrapolate changes in GPP due to a longer growing season length using the noted range in daily incremental increases in GPP. As such, productivity was defined as either the product of the scaled fCover value and the linear regression parameters or in terms of changes in growing season length. To determine the total change in annual GPP across the study regions, we weighted model predictions according to the grassland fraction within each CMIP5 raster cell for those cells showing a significant trend across at least half of all projections.

**Future projections.** We projected fCover forward until 2100 using global parameter values, for ten downscaled (~1/8°) CMIP5 models<sup>48</sup> (Supplementary Table 6) with the business-as-usual RCP 8.5 projections of temperature and precipitation covering the continental USA, southern Canada and northern Mexico (25.125° to 52.875° N; 124.625° to 67.000° W). We only considered pixels classified as more than 50% grassland cover (MODIS Land Cover classes 10 and 7, Supplementary Fig. 1). Phenological metrics such as the start of the season (SOS), the end of the season (EOS) and the growing season length (GSL) were calculated using a 10% threshold. To characterize intra-annual variability we identified four distinct grassland regional groupings (R1–R4), based on characteristics of

projected future changes in fCover. All grassland statistics are weighted according to their fractional coverage within each grid cell where applicable.

**Climate summaries and summarizing statistics:** We describe changes in climate scenario drivers as the differences ( $\Delta$ ) between the end (2090–2100) and the start (2010–2020) of the twenty-first century. We report changes in the mean annual precipitation (mm), mean annual temperature ( $^{\circ}\text{C}$ ), precipitation frequency and aridity index, along with changes in mean seasonal precipitation and temperature. Precipitation frequency was calculated as the change in median precipitation frequency for precipitation events exceeding 2 mm, with positive values indicating increased delays between precipitation events. The aridity index was calculated according to the United Nations Environment Programme directions as the ratio of mean annual precipitation to mean annual potential evapotranspiration<sup>49</sup>.

## References

31. Sonnentag, O. *et al.* Digital repeat photography for phenological research in forest ecosystems. *Agric. For. Meteorol.* **152**, 159–177 (2012).
32. Keenan, T. F. *et al.* Tracking forest phenology and seasonal physiology using digital repeat photography: a critical assessment. *Ecol. Appl.* **24**, 1478–1489 (2014).
33. Donohue, R. J., Roderick, M. L., McVicar, T. R. & Farquhar, G. D. Impact of  $\text{CO}_2$  fertilization on maximum foliage cover across the globe's warm, arid environments. *Geophys. Res. Lett.* **40**, 3031–3035 (2013).
34. Yan, W. & Hunt, L. An equation for modelling the temperature response of plants using only the cardinal temperatures. *Ann. Bot.* **84**, 607–614 (1999).
35. *Global Gridded Surfaces of Selected Soil Characteristics (IGBP-DIS)* (Global Soil Data Task Group, Oak Ridge National Laboratory Distributed Active Archive Center, accessed 15 April 2014).
36. Hargreaves, G. & Samani, Z. Reference crop evapotranspiration from ambient air temperature. *Am. Soc. Agric. Eng.* **1**, 96–99 (1985).
37. Michalsky, J. J. The astronomical Almanac's algorithm for approximate solar position (1950–2050). *Sol. Energy* **40**, 227–235 (1988).
38. Thornton, P. E. & Running, S. W. An improved algorithm for estimating incident daily solar radiation from measurements of temperature, humidity, and precipitation. *Agric. For. Meteorol.* **93**, 211–228 (1999).
39. Metropolis, N., Rosenbluth, A. W., Rosenbluth, M. N., Teller, A. H. & Teller, E. Equation of state by fast computing machines. *J. Chem. Phys.* **21**, 1087–1092 (1953).
40. Carlson, T. N. & Ripley, D. A. On the relation between NDVI, fractional vegetation cover, and leaf area index. *Remote Sens. Environ.* **62**, 241–252 (1997).
41. Grant, R. F., Baldocchi, D. D. & Ma, S. Ecological controls on net ecosystem productivity of a seasonally dry annual grassland under current and future climates: modelling with ecosys. *Agric. For. Meteorol.* **152**, 189–200 (2012).
42. Barr, A. G. *et al.* Inter-annual variability in the leaf area index of a boreal aspen-hazelnut forest in relation to net ecosystem production. *Agric. For. Meteorol.* **126**, 237–255 (2004).
43. Reichstein, M. *et al.* On the separation of net ecosystem exchange into assimilation and ecosystem respiration: review and improved algorithm. *Glob. Change Biol.* **11**, 1424–1439 (2005).
44. Zeri, M. *et al.* Carbon exchange by establishing biofuel crops in Central Illinois. *Agric. Ecosyst. Environ.* **144**, 319–329 (2011).
45. Scott, R. L., Hamerlynck, E. P., Jenerette, G. D., Moran, M. S. & Barron-Gafford, G. A. Carbon dioxide exchange in a semidesert grassland through drought-induced vegetation change. *J. Geophys. Res.* **115**, G03026 (2010).
46. Brunsell, N. A., Nippert, J. B. & Buck, T. L. Impacts of seasonality and surface heterogeneity on water-use efficiency in mesic grasslands. *Ecohydrology* **7**, 1223–1233 (2014).
47. Flanagan, L. B., Wever, L. A. & Carlson, P. Seasonal and interannual variation in carbon dioxide exchange and carbon balance in a northern temperate grassland. *Glob. Change Biol.* **8**, 599–615 (2002).
48. Brekke, L., Thrasher, B. L., Maurer, E. P. & Pruitt, T. *Downscaled CMIP3 and CMIP5 Climate Projections* (US Department of the Interior, Bureau of Reclamation, Technical Services Center, 2013).
49. *World Atlas of Desertification* 2nd edn (UNEP, 2002).